

A Mixture Fraction-Based Model for Evaporation, Pyrolysis and Char Conversion of Dilute Fuel Dispersions

M. N. Khan¹, Long Fei Zhao¹, M. J. Cleary¹, R. W. Bilger¹, O. T. Stein² and A. Kronenburg²

¹School of Aerospace, Mechanical and Mechatronic Engineering
 The University of Sydney, NSW 2006, Australia

²Institut für Technische Verbrennung
 Universität Stuttgart, Baden Wurttemberg 70174, Germany

Abstract

Relations for the heat and mass transfer between the dispersed and continuous phases in multiphase combustion are derived in terms of the mixture fraction. The theory is general and therefore applicable to both liquid and solid fuel dispersions. Evaporation, pyrolysis and char conversion are all considered with each process resulting in different boundary conditions at the phase interface. The model is being implemented in a CFD code. We validate the dispersion part of the code against data for two non-reacting dilute jets.

Introduction

Models for the turbulent combustion of gaseous fuels are widely reviewed in the literature [1], and among those, the mixture fraction-based models for non-premixed combustion are highly regarded for their accuracy and computational efficiency [2]. However, most practical combustion processes involve liquid or solid fuels in flows involving atomisation and dispersion, vaporisation, pyrolysis, and heterogeneous and homogeneous combustion. Each process is affected by turbulence. Just as the closure of turbulent gas-phase reaction rates is complicated by their non-linearity, so too is the closure of the turbulent heat and mass transfer rates between the continuous and dispersed phases. In the context of a single, evaporating liquid droplet, Spalding [3] derived heat and mass transfer relations both with and without gas-phase reactions. He showed that, for cases where combustion reactions are occurring, the transfer relations are greatly simplified when based on conserved scalars such as the mixture fraction and/or standardised enthalpy. Some contemporary spray combustion publications [5] use transfer relations which are, strictly speaking, only valid in the absence of gas-phase combustion. The implications of this inconsistency are untested.

Here we derive consistent, mixture fraction-based expressions for heat and mass transfer. Our starting point is the derivation of heat and mass transfer between a single isolated fuel particle and quiescent, gaseous surroundings. For the first time we extend the theory, already well known for evaporating liquid droplets, to mass transfer by pyrolysis and char conversion. The model is being implemented numerically in an LES code based on OpenFOAM with the aim of applying it to spray [7] and pulverised solid fuel [8] flames. As a first step we validate the modelling of the fuel particle dispersion by comparison to experimental data for non-reacting kerosene and coal cases.

Heat and Mass Transfer for an Isolated Fuel Particle

We start by considering simultaneous heat and mass transfer between a single, isolated liquid or solid fuel particle and an infinite, quiescent gaseous environment shown schematically in figure 1. We denote the fuel particle by 'D' (for dispersed phase) and the point in the gas remote from the particle as 'G'.

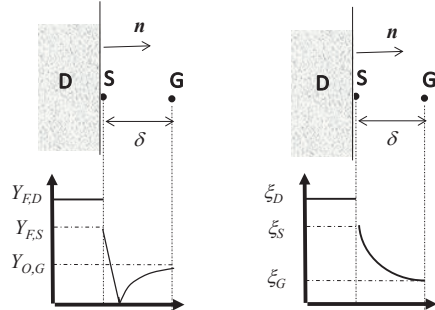


Figure 1: Schematic of (left) the mass fraction profile of reactive species, Y_F and Y_O and (right) the mixture fraction, ξ .

The point on the gas side of the phase interface is denoted by 'S'. The analysis is for one-dimensional heat and mass transfer which is a convenient simplification applicable to both spherical and long filament fuel particles. The outward normal vector is n . It is additionally assumed that gaseous heat and mass transfer are *quasi-steady* meaning that the timescale of transport in the gaseous layer is small relative to transport timescales in the dispersed phase. The left side of figure 1 shows the profile of an evaporative reactive fuel species, Y_F , which has a uniform value in the fuel particle, a surface discontinuity due to a *jump condition*, and diffusion to the reaction zone where it is consumed. On the outer side of the reaction zone an oxidiser species, Y_O , is shown. The diffusion-reaction equation for the fuel species is

$$\rho \mathcal{D} \frac{\partial^2 Y_F}{\partial n^2} - \rho v \frac{\partial Y_F}{\partial n} = W_F \quad (1)$$

where ρ is density, \mathcal{D} is diffusivity, v is the velocity due to Stefan flow and W_F is the reaction rate. The latter is non-linear making integration of equation (1) between the 'D' and 'G' states non-trivial. Turns [4] circumvents this by introducing an additional boundary condition at the reaction zone which is assumed to be infinitely thin. In practice, reactions proceed at finite rates resulting in broadened reaction zones which may even become broken due to intense turbulent mixing or quenching. A more general solution is obtained by considering conserved scalars such as the mixture fraction shown on the right side of figure 1. Conserved scalars are not affected by chemical reactions alleviating the above mentioned problem. Furthermore, the conserved scalar approach is better suited to the analysis of mass transfer by pyrolysis or heterogeneous char conversion, both of which are irreversible thermochemical processes. This is because we can define the mixture fraction and standardised enthalpy in the dispersed phase whereas $Y_{F,D}$ may be undefined.

The mixture fraction is defined as the normalisation of any conserved scalar, β :

$$\xi = \frac{\beta - \beta_0}{\beta_1 - \beta_0}. \quad (2)$$

where subscripts 0 and 1 represent the values in pure oxidiser and pure fuel, respectively. ξ has the same definition in both the dispersed and gas phases. For mass transfer from fuel particles without gas phase combustion, the mass fraction of the transferred species is a conserved scalar and it is natural to set $\beta = Y_F$. Under combustion conditions molecular species are not conserved but atomic elements are, so we use $\beta = Y_e$, where e can represent any element (assuming differential diffusivity is not important). The standardised enthalpies in the dispersed and gas phases are defined as

$$h_D = C_{p,D} (T_D - T^r) \quad (3)$$

$$h_G = \sum_{\alpha=1}^{N_s} \left[h_f^\alpha + \int_{T_r}^{T_G} C_{p,G} dT \right]_\alpha. \quad (4)$$

where C_p is the specific heat, T_r is a reference temperature and h_f is enthalpy of formation.

The energy and mass transfer equations in the diffusive layer are

$$\rho\alpha \frac{\partial^2 h}{\partial n^2} - \rho v \frac{\partial h}{\partial n} = 0 \quad (5)$$

$$\rho\mathcal{D} \frac{\partial^2 \xi}{\partial n^2} - \rho v \frac{\partial \xi}{\partial n} = 0. \quad (6)$$

where the thermal diffusivity, α , has been introduced. To obtain expressions for the heat and mass fluxes, \dot{Q}'' and \dot{m}'' , equations 5 and 6 are integrated twice with the aid of the phase interface boundary conditions shown schematically in figure 2 and defined mathematically by

$$\dot{Q}_D'' = \rho\alpha \frac{\partial h}{\partial n} \Big|_S - \dot{Q}_p'' + \dot{Q}_R'' \quad (7)$$

$$\dot{m}'' \xi_D = \rho v_S \xi_S - \rho \mathcal{D} \frac{\partial \xi}{\partial n} \Big|_S. \quad (8)$$

The boundary conditions incorporate heat fluxes for radiation, \dot{Q}_R'' , internal heating of the fuel particle, \dot{Q}_D'' and latent heat of phase change, \dot{Q}_p'' , which are balanced by conductive heat transfer from the gas phase. Following convention, radiation outwards from the fuel particle has a negative value.

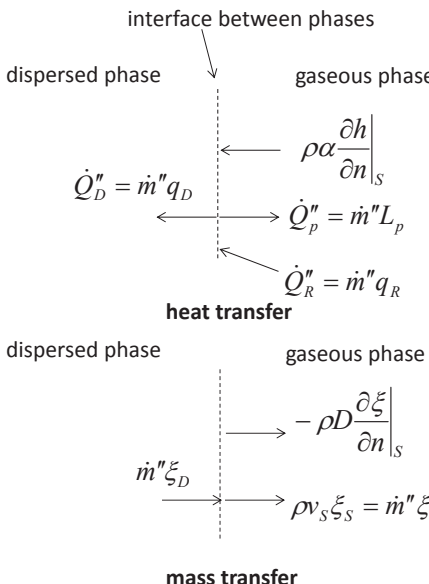


Figure 2: Heat and mass transfer interface boundary conditions.

After integration and some rearrangement we obtain

$$\dot{Q}'' = \dot{m}'' (L_p + q_D - q_R) \quad (9)$$

$$\dot{m}'' = \text{Nu} \frac{\rho\alpha}{L} \ln(1 + B_H) = \text{Sh} \frac{\rho\mathcal{D}}{L} \ln(1 + B_M) \quad (10)$$

where

$$B_H = \frac{h_G - h_S}{L_p + q_D - q_R} \quad (11)$$

$$B_M = \frac{\xi_G - \xi_S}{\xi_S - 1} \quad (12)$$

are the Spalding transfer numbers, L is the characteristic length scale of the phase interface (e.g. diameter for spherical particles). $\xi_D = 1$ has been used in the denominator of equation 12 without loss of generality. We have introduced Nu and Sh, the Nusselt and Sherwood numbers, to cover both quiescent and convective transfer environments. They are often correlated to Reynolds, Prandtl and Schmidt numbers and have lower limits of Nu=Sh=2 for quiescent conditions.

Models are required for q_R and q_D . Radiation should be modelled to suit the conditions; a simple solid body radiation may be sufficient in many cases. From the equality expressed in equation 10 the internal heating is given by

$$q_D = \frac{h_G - h_S}{(1 + B_M)^Z - 1} - L_p + q_R \quad (13)$$

where $Z = \text{Le}^{-1} \text{Sh}/\text{Nu}$ and $\text{Le} = \alpha/\mathcal{D}$ is the Lewis number.

Finally we require values for h and ξ at the 'S' and 'G' states. These are abstracted with information from the turbulent gas phase combustion model (e.g. MMC-LES [6] or CMC-LES [10]) which provides reactive species at the 'G' state. ξ_G is sampled randomly with an assumed β -PDF, the moments of which are obtained directly from the LES. ξ_S is found directly (pyrolysis) or indirectly from conditional averaging (evaporation and char conversion). For the latter, it is assumed that a species, i , is a unique function of the mixture fraction, $Y_i = f(\xi)$, where f is given by the gas-phase combustion model. The inverse function then gives $\xi_S = f^{-1}(Y_{i,S})$ with $Y_{i,S}$ being determined by the process dependent interface conditions (described for each process below). It is common to set $T_S = T_D$, where T_D is obtained from a simple lumped capacitance approach [5]. h_G and h_S are then obtained as functions of the mixture fraction and temperature.

Evaporation - apply the Clausius-Clapeyron phase equilibrium relation for the fuel species ($i = F$):

$$Y_{F,S} = \left[1 + \frac{MW_{\text{air}}}{MW_\alpha} \left(\frac{P}{P_F} - 1 \right) \right]^{-1} \quad (14)$$

where MW is molecular weight, P is total pressure and P_F is vapour pressure.

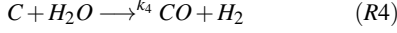
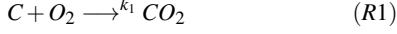
Pyrolysis - apply temperature dependent decomposition such as those given in [9] to obtain ξ_S directly

$$\xi_S = 1 + \frac{\xi_G - 1}{e^K} \quad (15)$$

where K is a pyrolysis species rate parameter.

Char conversion - apply surface kinetics of arbitrary complexity and solve iteratively for gaseous species mass fractions at the

interface. A demonstration is given for a simple four-step char combustion mechanism:



In the above k denotes a reaction rate coefficient. At high temperatures, typical of pulverised fuel combustion, the reactions R2 and R3 are dominant and we can greatly simplify our analysis - since the char is converted to CO only - by disregarding reactions R1 and R4. Making the assumption that the surface reaction kinetics are first order the CO mass flux is

$$\dot{m}_{CO}'' = \mathcal{K}_2 Y_{O_2,S} + 2\mathcal{K}_3 Y_{CO_2,S} \quad (16)$$

where

$$\mathcal{K}_2 = k_2 \frac{MW_{CO} MW_{mix,S}}{MW_{O_2}} \frac{P}{R_u T_S} \quad (17)$$

$$\mathcal{K}_3 = k_3 \frac{MW_{CO} MW_{mix,S}}{MW_{CO_2}} \frac{P}{R_u T_S}. \quad (18)$$

The mass fluxes of the other gaseous species involved in the heterogeneous reactions from the fuel particle are similarly given by kinetic relations

$$\dot{m}_{O_2}'' = -\frac{1}{2}\mathcal{K}_2 Y_{O_2,S} \quad (19)$$

$$\dot{m}_{CO_2}'' = -\mathcal{K}_3 Y_{CO_2,S}. \quad (20)$$

Finally the rate of carbon consumption is

$$\dot{m}_C = -(\mathcal{K}_2 Y_{O_2,S} + \mathcal{K}_3 Y_{CO_2,S}) A. \quad (21)$$

where A is the interface area. We now have five equations - (10), (16), (19), (20), (21) - and six unknowns - \dot{m}_{CO}'' , \dot{m}_{O_2}'' , \dot{m}_C , $Y_{O_2,S}$, $Y_{CO_2,S}$. One additional equation comes from the conservation of mass

$$\dot{m}_{CO}'' = \frac{\dot{m}_C}{A} + \dot{m}_{O_2}'' + \dot{m}_{CO_2}''. \quad (22)$$

Numerical Implementation

The model is being implemented in a new OpenFOAM C++ compatible LES code, called *mmcFoam*, which was recently developed at the University of Sydney. The object oriented code is structured with nested templates (i.e. generic code which is instantiated at runtime). Each level of the nested templates represents specific physics. For the fuel particles there are template levels for kinematics (i.e. momentum transfer), thermodynamics (i.e. heat transfer and physical properties), mass transfer and heterogeneous reactions. For the gas-phase turbulent combustion based on the MMC-LES model [6] there are template levels for stochastic transport, thermodynamics, mixing and homogeneous reactions. Our implementation retains all the generality of OpenFOAM allowing for structured and unstructured grids, numerous discretisation and integration schemes, and the full range of thermodynamic and kinetic flexibility.

As a first step, we validate the kinematic part of the fuel particle code. The Lagrangian equations governing the location and velocity each fuel particle are [5]

$$\frac{dx_i}{dt} = u_{D,i} \quad (23)$$

$$du_{D,i} = (a_{D,i} + g_i) dt + b_{D,i} d\omega_i. \quad (24)$$

The velocity of the inertial fuel particles is a response to drag forces imparted by the gas-phase and gravity. The deterministic acceleration is modelled as a relaxation to the filtered gas-phase velocity

$$a_{D,i} = \frac{\tilde{u}_{G,i} - u_{D,i}}{\tau} \quad (25)$$

where the timescale

$$\frac{1}{\tau} = \frac{3}{4} \frac{\rho_G}{\rho_D} \frac{C_d}{D} |\tilde{u}_G - u_D| \quad (26)$$

is a function of the drag coefficient (calculated for spherical particles) [11]

$$C_d = \frac{24}{Re} \left(1 + \frac{(Re)^{2/3}}{6} \right); \quad \text{for } 0 < Re < 1000 \\ = 0.424; \quad \text{for } Re \geq 1000 \quad (27)$$

In Eq.(24) $b_{D,i} d\omega_i$ is a stochastic term which simulates the sub-filter differential velocity. It generally has a very small effect in LES and may be neglected as a first approximation [10]. A complete version of Eq.(24) contains further terms for the effects of pressure gradient, the Basset force, and the Saffman and Magnus lift forces but these are usually small enough to be neglected. In return, the particles impart a momentum change on the gas-phase, appearing as a source term in the Navier-Stokes equation.

Results

Two non-reacting multiphase flows are simulated. The first is the non-reactive dispersion of kerosene (KS6) from the University of Sydney spray burner by Gounder et al. [7] while the second is the non-reactive dispersion of pulverised coal by Hwang et. al. [8]. For the kerosene case the 3D flow domain extends 104mm transversely by 320mm axially with a total of 466,560 cells. For the coal case the domain is 31mm transversely by 180mm axially with a total of 783,000 cells. In both cases zero gradient pressure boundary conditions are applied for the jet and coflow while fixed (total) pressure boundary conditions are at the domain sides and outlet. Realistic jet turbulent velocity boundary conditions are applied; for the kerosene case this is based on the exit plane experimental data, while for the coal case the settings reported in [12] are used.

Figure 3 shows axial and radial profiles of mean and rms particle velocity for the coal case. The simulations accurately capture the jet breakup point at about $z/D = 5$ and the subsequent decay. There is some underprediction of the mean about mid-way along the domain which is also clear in the radial profiles. The magnitude and trend for the rms is very well captured. Results for the kerosene case are shown in figure 4 and 5, for which results are further classified on particle size; 0-10 μm for the axial plot, and 10-20 and 40-50 μm for the radial results. Predictions are generally in good agreement with the data and importantly the slower rate of decay of the larger particles is correctly captured. Conversely to the coal case, there is overprediction of the mean at mid-way along the domain which is particularly noticeable at $z/D = 20$ in the radial plots. Additional simulations will be performed to determine the cause of this discrepancy.

Conclusions

A mixture fraction-based model is derived for heat and mass transfer in multiphase turbulent combustion. For the first time this model is extended to account for the combined effects of evaporation, pyrolysis and char conversion. The new model is being implemented into a CFD code which has been validated initially for non-reactive dispersion of both a kerosene spray

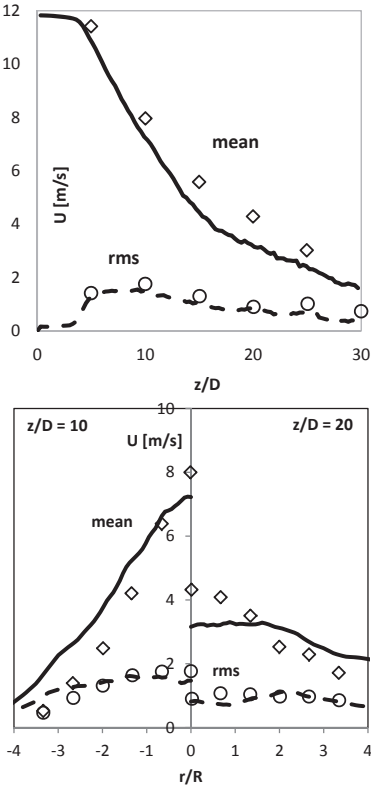


Figure 3: Axial (top) and two radial (bottom) profiles of mean and rms of particle velocity for the coal case. Symbols - experimental data [8]; lines - predictions.

and a coal case. Results are in good agreement with experimental data. Future work will focus initially on evaporating cases without combustion, followed by model validation for full combustion cases.

Acknowledgements

We acknowledge support from the ARC under grant number DP130100763 and the DAAD under postdoctoral fellowship 91510616-50015191. Thanks to G. Olenik for advice on boundary conditions and for the turbulent inflow generator code.

References

- [1] Bilger, R.W., Pope, S.B., Bray, K.N.C. and Driscoll, J.F., *Proc. Combust. Inst.*, **30**, 2005, 31–42.
- [2] Klimenko, A.Y. and Bilger, R.W., *Prog. Energy Combust. Sci.*, **25**, 1999, 595–687.
- [3] Spalding, D.B., *Some Fundamentals of Combustion*, Butterworth Scientific Publications, London, 1955.
- [4] Turns, S.R., *An Introduction to Combustion. Concepts and Applications*, McGraw-Hill, Singapore, 2012.
- [5] Jones, W.P. Lyra, S. and Navarro-Martinez, S., *Combust. Flame*, **159**, 2012, 1539–1561.
- [6] Ge, Y., Cleary, M.J. and Klimenko, A.Y., *Proc. Combust. Inst.*, **34**, 2013, 1325–1332.
- [7] Gounder, J.D., Kourmatzis, A. and Masri, A.R., *Combust. Flame*, **159**, 2012, 3372–3397.
- [8] Hwang, S.M., *Energ. Fuel.*, **19**, 2005, 382–392.
- [9] Solomon, P.R., Fletcher, T.H. and Pugmire, R.J., *Fuel*, **72**, 1993, 587–597.
- [10] Ukai, S., Kronenburg, A. and Stein, O.T., *Proc. Combust. Inst.*, **34**, 2013, 1643–1650.
- [11] Yuen, M.C. and Chen, L.W., *Combust. Sci. Technol.*, **14**, 1976, 147–154.
- [12] Stein, O.T., Olenik, G., Kronenburg, A., Cavallo Marincola, F., Franchetti, B.M., Kempf, A.M., Ghiani, M., Vassellari, M. and Hasse, C., *Flow, Turbul. Combust.*, **90**, 2013, 859–884.

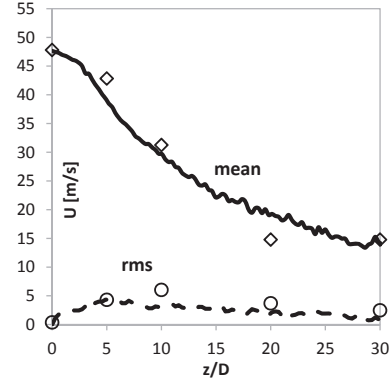


Figure 4: Axial profiles of velocity mean and rms for droplets in the range 0 - 10 μm for the kerosene case. Symbols - experimental data [7]; lines - predictions.

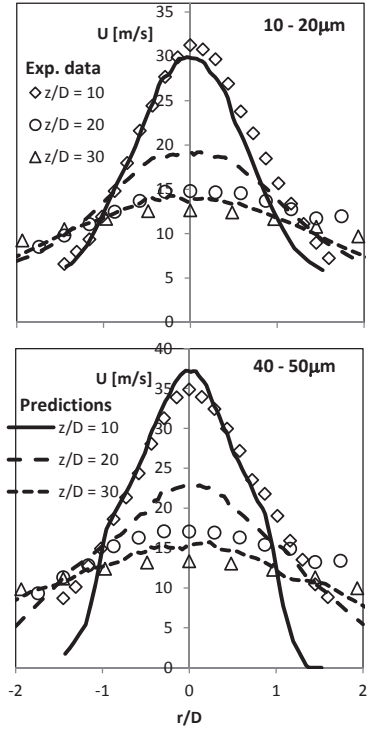


Figure 5: Radial profiles at three axial stations of size conditioned mean droplet velocity for the kerosene case. Symbols - experimental data [7]; lines - predictions.